Jurnal Presipitasi
Media Komunikasi dan Pengembangan Teknik Lingkungan
e-ISSN: 2550-0023

Vol 23, No 3, 2026,
Article available at homepage presipitasi

Original Research Article

Spatial Mapping and Hotspot Identification of Mercury Contamination in Former Artisanal Gold Mining Soil Using Ordinary Kriging

M. Akbari Danasla[1*], Anjas Jevi Surya[1], Yohanna Tresna Oktavia Sigiro[1], Muhammad Rizky Saputra[1], Anja Firash Ipri Danasla[2], Setyo Budi Kurniawan[3,4]

[1]Department of Mining Engineering, Faculty of Technology Industry, Institut Teknologi Sumatera, Lampung-35365, Indonesia

[2]Sekretariat DPRD Kota Pekanbaru, Pekanbaru Riau, Indonesia

[3]Research Center for Environmental and Clean Technologies, National Research and Innovation Agency (BRIN), Jakarta Pusat 10340, Indonesia

[4]Faculty of Bioresource and Food Industry, Universiti Sultan Zainal Abidin, Besut Campus, 22200 Besut, Malaysia

* Corresponding Author, email: m.danasla@ta.itera.ac.id

Copyright ©2026 by Authors,
Published by Environmental Engineering Department,
Faculty of Engineering, UniversitasDiponegoro
This open accessarticle is distributed under a
Creative Commons Attribution 4.0 International License

Abstract

Mercury contamination is a persistent environmental legacy of artisanal and small-scale gold mining (ASGM), yet effective remediation is often hindered by limited knowledge of its spatial distribution. This study aimed to characterize the spatial distribution of mercury contamination in soils within a former ASGM area using geostatistical analysis, with particular emphasis on identifying contamination hotspots and examining their relationship with local topographic conditions. Thirty georeferenced surface soil samples were analyzed for aqua-regia-extractable mercury using Cold Vapor Atomic Absorption Spectrophotometry (CV-AAS). Mercury concentrations ranged from 0.18 to 89.82 mg kg^{-1}, with a mean of 10.18 mg kg^{-1}, and 60% of the samples exceeded the critical threshold of 0.50 mg kg^{-1}. The dataset exhibited high spatial heterogeneity, with a coefficient of variation of 2.20 and contamination dominated by localized hotspots. Among the evaluated semivariogram models, the Gaussian model yielded the lowest RMSE (13.96) and was selected for Ordinary Kriging interpolation. The resulting map identified distinct mercury hotspots associated with historical ore-processing areas. These findings demonstrate that mercury contamination is highly localized and support hotspot-based remediation as a more effective strategy than uniform site-wide treatment, providing a practical framework for environmental monitoring and post-mining land management.

Keywords: ASGM; environmental remediation; mercury contamination; soil pollution

1. Introduction

Artisanal and small-scale gold mining (ASGM) remains a major source of mercury release into the environment, particularly in developing regions where mining is often conducted with simple technology and limited waste management practices (Wibowo et al., 2022). Mercury is widely used in gold extraction because of its ability to form amalgam with gold. Still, improper handling, discharge of

tailings, and the absence of containment systems may lead to long-term contamination of soil, water, and sediment (Ngatijo et al., 2021). Once released into the environment, mercury can persist for extended periods, undergo transformation, migrate via surface runoff, and accumulate in low-lying areas (Ridwan et al., 2021; Uddin et al., 2024). Therefore, former ASGM sites require continuous environmental assessment, especially in areas where mining activities have been abandoned but residual contamination may still pose ecological and human health risks.

Soil contamination by mercury in ASGM areas is often spatially heterogeneous because contaminant distribution is influenced by several local factors, including the locations of ore-processing activities and tailings disposal sites, soil properties, surface runoff, and topographic variation (Abdelaal et al., 2023). Conventional soil assessment based solely on individual sampling points is useful for determining mercury concentrations at specific locations (Gosar et al., 2016). Still, it may not adequately capture the spatial pattern of contamination across the entire affected area. Because mercury concentrations in contaminated soils can exhibit substantial spatial heterogeneity, a geostatistical approach is particularly useful for characterizing spatial dependence and predicting concentrations at unsampled locations (Goovaerts, 1999; Imo et al., 2018). For this reason, geostatistical approaches have increasingly been used in environmental contamination studies to estimate contaminant distributions between sampling points and to identify potential hotspot zones. Among these methods, Ordinary Kriging is widely used because it accounts for spatial autocorrelation via variogram modelling and produces a continuous prediction surface from discrete sampling data.

Although several studies have reported mercury contamination in ASGM-affected environments (Abdelaal et al., 2023; Danasla et al., 2025), site-specific spatial assessments remain important because contamination patterns can vary substantially between locations. In many former mining areas, environmental management is often constrained by insufficient spatial information on where mercury accumulates and which zones should be prioritized for remediation. Previous studies have applied spatial and geostatistical approaches to characterize mercury contamination in mining-affected environments. For example, Dołęgowska & Michalik, (2019) combined GIS-based geostatistical mapping with geochemical and multivariate analyses to delineate Hg distribution and relate elevated concentrations to historical mining activities in post-mining areas of Poland. Similarly, previous study applied indicator kriging and sequential Gaussian simulation at an abandoned Hg-mining site in Spain to estimate the spatial probability of exceeding contamination thresholds (Boente et al., 2019). Moreover, the relationship between spatial mercury distribution and local terrain conditions is not always clearly described, even though surface runoff and slope direction may influence contaminant transport and deposition. This limitation highlights the need for an integrated assessment that combines laboratory-based mercury measurement, statistical analysis, and geostatistical mapping to support environmental risk evaluation in post-mining landscapes.

This study aims to evaluate the spatial distribution of mercury contamination in soil from a former artisanal gold mining area in Sidomekar Village, South Lampung, Indonesia. To achieve this general objective, the study specifically seeks to: (1) determine the concentration range and statistical characteristics of mercury in soil samples collected across the study area; (2) evaluate alternative variogram models and select the model that provides the most appropriate representation of spatial dependence; (3) generate a continuous spatial distribution map of soil mercury concentrations using Ordinary Kriging; and (4) delineate potential contamination hotspots and examine their possible relationship with local topographic conditions. The resulting spatial information is expected to support site-specific environmental monitoring, remediation prioritization, and risk communication for communities surrounding former ASGM areas.

2. Materials and Methods

2.1 Study Area

The study was conducted in a former ASGM area located in Sidomekar Village, South Lampung Regency, Lampung Province, Indonesia (approximately 105.398° E and 5.563° S). The site is an abandoned mercury amalgamation area where gold extraction was carried out intensively prior to mine closure. Although mining activities have ceased, no formal environmental remediation has been implemented, allowing residual mercury contamination to persist in the surrounding soils. The study area is characterized by gently undulating terrain surrounded by secondary vegetation and agricultural land. Historical ore processing and tailings disposal were concentrated within a relatively small area, making the site suitable for evaluating localized mercury contamination and spatial variability. The geographic coordinates of all sampling locations were referenced to the Universal Transverse Mercator (UTM) coordinate system using the WGS 84 datum for subsequent spatial analysis.

2.2 Soil Sampling and Sample Handling

Soil sampling and sample handling were conducted with reference to the ISO 18400 series for soil-quality investigations, particularly ISO 18400-101:2017, ISO 18400-102:2017, ISO 18400-105:2017, and ISO 18400-203:2018. These standards provide guidance on the development of sampling plans, selection and application of soil-sampling techniques, sample handling and transport, and investigation of potentially contaminated sites. Surface soil samples were collected from the former ASGM site using a purposive spatial sampling approach designed to represent areas with different potential levels and sources of Hg contamination. Sampling locations were selected based on evidence of previous mining and processing activities and included suspected former amalgamation sites, tailings disposal areas, surface-runoff pathways, and surrounding areas potentially affected by Hg dispersion. Such site-specific sampling is consistent with the investigation of potentially contaminated land, for which sampling locations may be selected according to previous land use, suspected contaminant sources, topography, and other site characteristics (ISO 18400-101:2017; ISO 18400-203:2018).

A total of 30 sampling points were established across the study area (Figure 1). At each sampling point, surface litter, stones, roots, and other coarse materials were removed before sample collection. Approximately 500 g of soil was collected from the upper 0–20 cm layer using clean stainless-steel sampling equipment. The selection of the 0–20 cm interval was intended to characterize the surface soil most directly influenced by historical mining activities, Hg deposition, and subsequent surface-transport processes. Each sample was immediately transferred into a clean, labelled polyethylene sampling bag and transported to the laboratory for subsequent preparation and analysis. Sampling equipment was thoroughly cleaned between sampling locations to minimize cross-contamination. Sample collection, handling, packaging, and transport followed the general principles described in ISO 18400-102:2017 and ISO 18400-105:2017. The geographic coordinates of each sampling point were recorded using a handheld Global Positioning System (GPS) receiver with an estimated positional accuracy of approximately ±3–5 m.

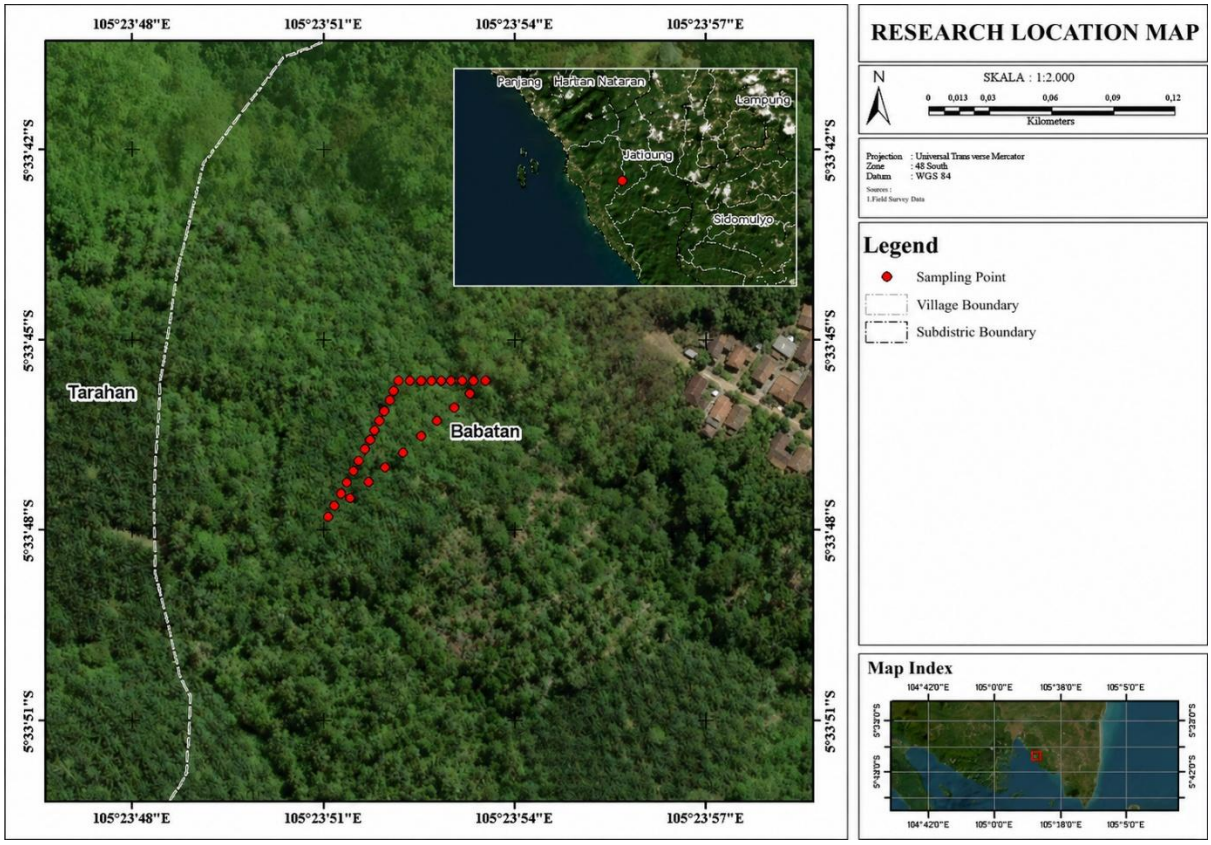


Figure 1. Location of collected soil

2.3 Sample Preparation and Acid Digestion

Soil samples were air-dried under ambient laboratory conditions (25–28 °C) until constant weight was achieved. Air drying at relatively low temperature was selected instead of high-temperature oven drying to minimize potential alteration or loss of volatile Hg species during sample preparation (Hojdová et al., 2015). The dried samples were gently disaggregated using a porcelain mortar and pestle, homogenized, and passed through a 2-mm stainless-steel sieve to remove gravel, roots, and other coarse materials.

Aqua-regia digestion was performed with reference to ISO 54321:2020 for the determination of aqua-regia-soluble elements in soil, including Hg. Approximately 0.50 g of homogenized soil was accurately weighed into an acid-cleaned digestion vessel. Freshly prepared aqua regia, consisting of concentrated hydrochloric acid (HCl, 37%) and nitric acid (HNO_3, 65%) at a volume ratio of 3:1, was then added. The samples were digested under controlled heating at approximately 95 °C for 2 h to facilitate the extraction of Hg associated with the soil matrix. After digestion, the samples were allowed to cool to room temperature, filtered when necessary, and diluted to a known volume with deionized water prior to instrumental determination. The resulting Hg concentrations therefore represent the aqua-regia-extractable fraction under the applied digestion conditions rather than necessarily the complete decomposition of the soil matrix (ISO 54321:2020). Mercury determination in aqua-regia soil extracts was conducted following the general principles of ISO 16772:2004.

2.4 Mercury Determination by Cold Vapor Atomic Absorption Spectrophotometry

Mercury concentrations in the aqua-regia soil extracts were determined by Cold Vapor Atomic Absorption Spectrophotometry (CV-AAS) using a Thermo Scientific™ iCE™ 3500 Atomic Absorption Spectrometer (Thermo Fisher Scientific, Cambridge, UK) equipped with a hydride/vapor generation configuration. The analysis was performed following the general principles of ISO 16772:2004 and US EPA

Method 7471B. The analytical principle involved the chemical reduction of dissolved mercury ions to elemental mercury (Hg^0), followed by separation of the volatile Hg^0 from the liquid phase and its transport into the absorption cell by a carrier gas. Mercury absorbance was measured at the Hg resonance wavelength of 253.7 nm.

2.5 Quality Assurance and Quality Control

Quality assurance and quality control (QA/QC) procedures were implemented throughout sample preparation and instrumental determination of mercury with reference to the quality-control principles described in US EPA SW-846 Method 7471B and ISO/IEC 17025:2017. Instrument calibration was performed using at least five mercury calibration standards covering the expected concentration range of the samples. Calibration curves were accepted when the coefficient of determination (R^2) was greater than 0.995, according to the laboratory's predefined acceptance criterion. Procedural blanks were included with each analytical batch to assess potential contamination arising from reagents, digestion, sample preparation, and instrumental analysis. Duplicate samples were analyzed to evaluate analytical precision, while calibration verification standards were measured periodically during the analytical sequence to confirm that instrument response remained stable. These procedures are consistent with US EPA Method 7471B, which recommends the use of method blanks, laboratory control samples, matrix spikes or duplicates, and periodic verification of the calibration response during mercury analysis.

Mercury analysis was performed by an external analytical laboratory. The samples were submitted after preparation and digestion, and the authors received the final reported mercury concentrations together with information on the analytical technique and instrumentation used. According to the analytical information provided by the laboratory, mercury determination was conducted using Cold Vapor Atomic Absorption Spectrophotometry (CV-AAS) with a Thermo Scientific™ iCE™ 3500 Atomic Absorption Spectrometer. The laboratory applied its routine internal quality-control procedures during instrumental analysis.

However, the complete raw QA/QC documentation generated during the analytical run, including individual procedural-blank results, duplicate precision, calibration-verification recoveries, certified-reference-material or matrix-spike recoveries, and method-specific LOD and LOQ values, was not included in the analytical report available to the authors. Therefore, these numerical parameters are not reported retrospectively in the present study. All mercury concentrations used in the statistical and geostatistical analyses correspond to the final analytical results reported by the external laboratory. The limited availability of detailed analytical QA/QC records is acknowledged as a methodological limitation of the present study.

2.6 Statistical and Geostatistical Analysis

Descriptive statistics were used to characterize the distribution and variability of aqua-regia-extractable Hg concentrations across the study area. The calculated statistics comprised the minimum, maximum, arithmetic mean, median, first quartile (Q_1), third quartile (Q_3), standard deviation, variance, coefficient of variation, skewness, and kurtosis. A frequency distribution was also constructed to describe concentration heterogeneity among the sampling locations.

Potential statistical outliers were identified using the interquartile range (IQR) method. The IQR was defined as:

$$IQR = Q_3 - Q_1$$

where Q_1 and Q_3 denote the first and third quartiles, respectively. An observation was classified as an upper outlier when it exceeded the following threshold:

$$Q_3 + 1.5(IQR)$$

Exceptionally high Hg concentrations may represent genuine contamination hotspots rather than analytical errors; therefore, observations identified as outliers were retained in the geostatistical

analysis. Their contribution to the cumulative measured Hg concentration was quantified to assess the extent to which localized high-concentration observations influenced the dataset.

Spatial dependence and the prediction of Hg concentrations were evaluated using Ordinary Kriging (OK). The experimental semivariogram was calculated with the classical Matheron estimator:

$$\gamma(h) = [1/(2N(h))] \sum_{i=1}^{N(h)} [Z(x_i) - Z(x_i + h)]^2$$

where $\gamma(h)$ is the semivariance at lag distance h; $N(h)$ is the number of observation pairs separated by approximately h; $Z(x_i)$ is the measured Hg concentration at location x_i; and $Z(x_i + h)$ is the measured Hg concentration at a location separated from x_i by the lag vector h.

Three theoretical semivariogram models—Spherical, Exponential, and Gaussian—were fitted to the experimental semivariogram. Model selection was not based solely on the minimum root mean square error (RMSE). Predictive performance was assessed by leave-one-out cross-validation using mean error (ME), RMSE, mean standardized error (MSE), root mean square standardized error (RMSSE), and agreement between observed and cross-validated predicted Hg concentrations. Models with ME and MSE close to zero, RMSSE close to 1, and comparatively low RMSE were regarded as having better predictive performance. The final model was selected by considering the complete set of cross-validation diagnostics together with the plausibility of the fitted spatial structure.

Spatial prediction was performed using the Ordinary Kriging estimator:

$$Z^*(x_0) = \sum_{i=1}^{n} \lambda_i Z(x_i)$$

where $Z^*(x_0)$ is the predicted Hg concentration at unsampled location x_0; λ_i is the kriging weight assigned to the observation at location x_i; $Z(x_i)$ is the measured Hg concentration at x_i; and n is the number of neighboring observations used for prediction. The kriging weights were constrained to sum to one, thereby ensuring an unbiased estimate.

Because the Hg dataset exhibited strong positive skewness and several extremely high concentrations, a sensitivity analysis was also performed using logarithmically transformed Hg concentrations. All sampling locations were retained. Experimental semivariograms were reconstructed for the transformed dataset and fitted with the same Spherical, Exponential, and Gaussian models used for the untransformed data. Cross-validation performance and the spatial persistence of the principal high-concentration zones were then compared between the two analyses. This sensitivity analysis assessed whether the main spatial interpretation was disproportionately controlled by the highest Hg concentrations.

Because the 30 sampling locations were selected purposively and were not uniformly distributed across the mapped extent, interpretation of the kriging results was restricted to the spatial domain adequately supported by the observations. The prediction surface was clipped to this sampling-supported domain, and predictions outside it were excluded from quantitative interpretation. This restriction minimized unsupported extrapolation into areas distant from measured locations, particularly beyond the effective spatial-correlation range indicated by the fitted semivariogram.

Geographic coordinates and Hg concentration data were integrated in a Geographic Information System (GIS) for spatial analysis and map production. Sampling locations were projected in the Universal Transverse Mercator coordinate system using the WGS 84 datum. Semivariogram modelling, Ordinary Kriging, leave-one-out cross-validation, spatial interpolation, contour generation, and thematic mapping were conducted in ArcGIS 10.8. The resulting prediction surfaces were used primarily to delineate spatial patterns and potential Hg hotspot zones within the sampling-supported domain and to examine their spatial relationships with historical mining activities and surrounding landscape features.

3. Results and Discussion

3.1 Mercury Concentration and Contamination Status of Soil Samples

Mercury concentrations measured in the 30 surface soil samples collected from the former ASGM area exhibited substantial spatial variability, ranging from 0.18 to 89.82 mg kg^{-1} (Table 1). This wide concentration range indicates that mercury contamination was highly heterogeneous across the study

area rather than uniformly distributed. Such variability is characteristic of abandoned ASGM sites, where mercury contamination is strongly influenced by the locations of historical amalgamation activities, tailings disposal practices, and subsequent redistribution through surface runoff and erosion. Previous studies have similarly reported highly heterogeneous mercury distributions in former ASGM environments, reflecting the localized nature of mercury release during gold extraction processes (El Hadi et al., 2026; Szponar et al., 2025)

Table 1. Mercury concentration in soil samples collected from the former ASGM area

Hg concentration (mg/kg)	Longitude	Latitude	Contamination category
2.28	105.3977278	-5.562894445	Above critical threshold
78.17	105.3975222	-5.563275	Above critical threshold
40.74	105.3982056	-5.562677778	Above critical threshold
0.83	105.3978278	-5.562677777	Above critical threshold
16.47	105.3977653	-5.562810039	Above critical threshold
89.82	105.3975482	-5.56322426	Above critical threshold
0.55	105.3976965	-5.563123782	Above critical threshold
0.36	105.3979257	-5.562922575	Critical range
0.64	105.3981074	-5.562676881	Above critical threshold
0.36	105.3980709	-5.562794186	Critical range
1.27	105.3975769	-5.563173977	Above critical threshold
0.43	105.398059	-5.562676913	Critical range
1.02	105.3979983	-5.562857423	Above critical threshold
2.05	105.3979204	-5.562677605	Above critical threshold
0.49	105.3976182	-5.563190853	Critical range
1.02	105.3981377	-5.562736697	Above critical threshold
0.47	105.3976556	-5.563029118	Critical range
0.28	105.3976305	-5.563075808	Normal range
0.37	105.397771	-5.563060544	Critical range
0.34	105.397683	-5.562980032	Critical range
1.08	105.3978493	-5.562991559	Above critical threshold
0.18	105.3981528	-5.56267685	Normal range
0.22	105.3979628	-5.562678175	Normal range
18.62	105.3978071	-5.562721452	Above critical threshold
0.99	105.398013	-5.562678141	Above critical threshold
0.81	105.3978756	-5.562678234	Above critical threshold
31.8	105.3977868	-5.562765745	Above critical threshold
0.42	105.3977069	-5.562934541	Critical range
0.49	105.3976031	-5.56312609	Critical range
12.78	105.3977463	-5.562854332	Above critical threshold

Note: For descriptive comparison, Hg concentrations were evaluated against the Indonesian soil environmental-health reference value of 0.30 mg kg^{-1} specified in Regulation of the Minister of Health of the Republic of Indonesia No. 2 of 2023. Samples were therefore grouped as ≤0.30 mg kg^{-1} and >0.30 mg kg^{-1}. Because the present study quantified aqua-regia-extractable Hg rather than rigorously defined total Hg, this comparison is used as a screening reference and should not be interpreted as a direct regulatory compliance assessment.

Based on the contamination classification adopted in this study, 18 samples (60%) exceeded the critical threshold of 0.50 mg kg^{-1}, whereas nine samples (30%) were classified within the critical range

(0.30–0.50 mg kg^{-1}), and only three samples (10%) remained within the normal concentration range (<0.30 mg kg^{-1}) (Table 2). The predominance of samples exceeding the critical threshold demonstrates that mercury contamination remains widespread despite the cessation of mining activities. This finding highlights the long-term environmental persistence of mercury in soil systems, where mercury can strongly associate with fine mineral particles and soil organic matter, thereby limiting its mobility while allowing contamination to persist over extended periods. The prolonged persistence of mercury in abandoned mining environments has been widely recognized as one of the principal environmental challenges associated with ASGM activities (Moreno-Brush et al., 2020; Mulenga et al., 2024)

Table 2. Classification of mercury contamination levels in soil samples

Contamination category	Hg concentration range (mg/kg)	Number of samples	Percentage (%)	Mean Hg concentration (mg/kg)
Normal range	0.01–0.30	3	10	0.23
Critical range	>0.30–0.50	9	30	0.41
Above critical threshold	>0.50	18	60	16.72
Total	—	30	100	—

Although the majority of sampling locations were classified as contaminated, mercury concentrations were not evenly distributed throughout the study area. Several sampling points contained exceptionally high mercury concentrations, including 89.82, 78.17, 40.74, 31.80, and 18.62 mg kg^{-1}, whereas most remaining samples contained concentrations below 2 mg kg^{-1}. This pronounced contrast suggests that mercury contamination originated primarily from localized point sources rather than diffuse environmental deposition. These high-concentration locations most likely correspond to former ore-processing or amalgamation sites where elemental mercury was directly used during gold extraction, in line with the previous study (Carling et al., 2013). Consequently, residual mercury accumulated within relatively confined areas and remained detectable long after mining activities had ceased.

The observed concentration gradient from highly contaminated locations to surrounding areas also suggests that secondary transport processes have influenced the current mercury distribution. Following the abandonment of mining activities, mercury associated with soil particles may have been redistributed via surface runoff, erosion, and sediment transport, resulting in gradual dilution with increasing distance from the sources of contamination. Similar spatial redistribution patterns have frequently been documented in former ASGM landscapes, where the combined effects of anthropogenic activities and local geomorphological conditions generate distinct contamination gradients across relatively small spatial scales. Mercury migration controlled by topography and hydrological processes has been reported as a major factor governing contaminant redistribution in post-mining environments (Cacciuttolo et al., 2023; Chen et al., 2026)

The contamination classification further demonstrates that relatively few highly contaminated locations contribute disproportionately to the overall mercury burden within the study area. This characteristic has important implications for environmental management because remediation efforts may be more effective when focused on localized contamination hotspots rather than uniformly treating the entire site. Identifying these highly contaminated zones therefore represents an essential step toward developing cost-effective remediation strategies, optimizing environmental monitoring programs, and minimizing potential ecological and human exposure risks.

3.2 Descriptive Statistics and Distribution Pattern of Mercury Contamination

Descriptive statistical analysis revealed that mercury concentrations in the former ASGM area exhibited an extremely heterogeneous distribution (Table 3). Mercury concentrations ranged from 0.18 to 89.82 mg kg^{-1}, with an arithmetic mean of 10.18 mg kg^{-1}, substantially exceeding the median value of 0.82 mg kg^{-1}. The considerable difference between the mean and median indicates that the dataset was strongly influenced by a limited number of exceptionally high mercury concentrations. Such disparity is characteristic of positively skewed environmental contamination data, in which localized hotspots contribute disproportionately to the overall contaminant burden.

Table 3. Descriptive statistics of mercury concentration in soil samples

Parameter	Value
Minimum Value	0.18
Maximum Value	89.82
Mean	10.18
Median	0.82
1st Quartile (Q1)	0.42
3rd Quartile (Q3)	2.22
Standard Deviation	22.39
Variance	501.43
Coefficient of Variation (CV)	2.2
Skewness	2.76
Kurtosis	7.27
N	30

The coefficient of variation (CV) reached 2.20, indicating extremely high spatial variability in mercury concentration throughout the study area. According to commonly accepted classifications of environmental datasets, coefficients of variation exceeding 1.0 generally indicate substantial spatial heterogeneity attributable to localized contamination sources rather than natural geochemical variation. The high variability observed in this study therefore suggests that mercury distribution is primarily controlled by historical mining activities instead of regional background concentrations. Similar patterns of elevated variability have frequently been reported in former ASGM areas where amalgamation was conducted at multiple localized processing sites (Donkor et al., 2024; Yoshimura et al., 2021)

The distribution of mercury concentrations was further characterized by a skewness value of 2.76 and a kurtosis value of 7.27, demonstrating a markedly non-normal distribution with a pronounced right tail. Positive skewness indicates that most sampling locations contained relatively low mercury concentrations, whereas a small number of locations exhibited extremely elevated values. Meanwhile, the high kurtosis reflects the presence of unusually extreme observations compared with a normal distribution, suggesting localized enrichment rather than gradual concentration changes across the landscape. Such statistical characteristics are commonly observed in contaminated soils where anthropogenic inputs dominate over natural geochemical processes. Mercury concentrations in mining-degraded soils commonly exhibit substantial spatial variability and non-normal distributions, reflecting the localized release, redistribution, and retention of Hg within mine spoils, processing areas, and downstream depositional environments (Becerra-Lira et al., 2024; Thiombane et al., 2023). Other studies have also shown that highly skewed mercury datasets are typical of abandoned mining environments because contamination is generally concentrated around former processing facilities and waste disposal sites, creating localized contamination hotspots with concentrations that decline rapidly with distance from the source (Eckley et al., 2020; Kocman et al., 2013).

The frequency distribution provides additional insight into the contamination pattern (Table 4). More than half of the sampling locations (56.7%) contained mercury concentrations below 1.0 mg kg^{-1},

whereas only four samples (13.4%) exceeded 20 mg kg^{-1}. Despite representing a relatively small proportion of the dataset, these highly contaminated samples accounted for the majority of the total mercury inventory within the study area. This finding indicates that mercury contamination is spatially concentrated rather than uniformly dispersed, supporting the hypothesis that historical amalgamation activities generated localized contamination hotspots.

Table 4. Frequency distribution of mercury concentration in soil samples

Hg concentration interval (mg/kg)	Number of samples	Percentage (%)	Mean Hg within class (mg/kg)	Cumulative Hg concentration (mg/kg)
≤0.30	3	10.0	0.23	0.68
>0.30–0.50	9	30.0	0.41	3.73
>0.50–1.00	5	16.7	0.76	3.82
>1.00–5.00	6	20.0	1.45	8.72
>5.00–20.00	3	10.0	15.96	47.87
>20.00–50.00	2	6.7	36.27	72.54
>50.00	2	6.7	84.00	167.99
Total	30	100.0	—	305.35

Outlier analysis using the interquartile range (IQR) method further confirmed localized mercury enrichment (Table 5). The calculated upper outlier threshold was 4.92 mg kg^{-1}, above which seven sampling locations (23.3%) were identified as statistical outliers. Although these samples represented less than one-quarter of the total observations, they collectively contributed 94.5% of the cumulative measured mercury concentration. Consequently, excluding these outliers reduced the arithmetic mean mercury concentration from 10.18 to only 0.74 mg kg^{-1}, demonstrating the overwhelming influence of a limited number of highly contaminated locations on the overall dataset.

Table 5. Outlier diagnostic based on interquartile range

Parameter	Value
Q1 (mg/kg)	0.42
Q3 (mg/kg)	2.22
IQR (mg/kg)	1.80
Upper outlier threshold, Q3 + 1.5 × IQR (mg/kg)	4.92
Number of samples above outlier threshold	7
Percentage of outlier samples (%)	23.3
Cumulative Hg concentration of outlier samples (mg/kg)	288.40
Contribution of outlier samples to cumulative measured Hg (%)	94.5
Mean Hg concentration including all samples (mg/kg)	10.18
Mean Hg concentration excluding outlier samples (mg/kg)	0.74

The pronounced influence of these outlier samples suggests that mercury contamination within the study area is dominated by discrete point sources rather than diffuse contamination processes. From an environmental perspective, this finding is particularly important because it indicates that the majority of the mercury burden is concentrated within relatively small portions of the former mining area. Similar contamination structures have been documented in abandoned ASGM sites worldwide, where mercury released during amalgamation remains highly localized due to limited post-depositional mobility and strong adsorption onto fine soil particles. Localized mercury enrichment associated with historical ore-processing activities has consistently been recognized as a defining characteristic of former ASGM environments (Esdaile and Chalker, 2018; Kocman et al., 2013)

The statistical characteristics observed in this study also have important implications for subsequent geostatistical analysis. Highly skewed datasets with distinct contamination hotspots often violate the assumptions of spatial stationarity required for interpolation and may strongly influence semivariogram construction. Nevertheless, these extreme values should not be removed because they represent genuine environmental conditions rather than analytical errors. Instead, retaining the outliers allows Ordinary Kriging to capture the actual spatial variability of mercury contamination and facilitates more realistic identification of contamination hotspots requiring remediation.

3.3 Variogram Model Evaluation and Spatial Dependence of Mercury

Understanding the spatial dependence of mercury concentrations is essential for selecting an appropriate interpolation model and accurately characterizing contamination patterns across the former ASGM site. Experimental semivariograms were therefore fitted using three commonly used theoretical models: Spherical, Exponential, and Gaussian. The corresponding model parameters and prediction errors are summarized in Table 6, while the fitted semivariograms are presented in Figure 2.

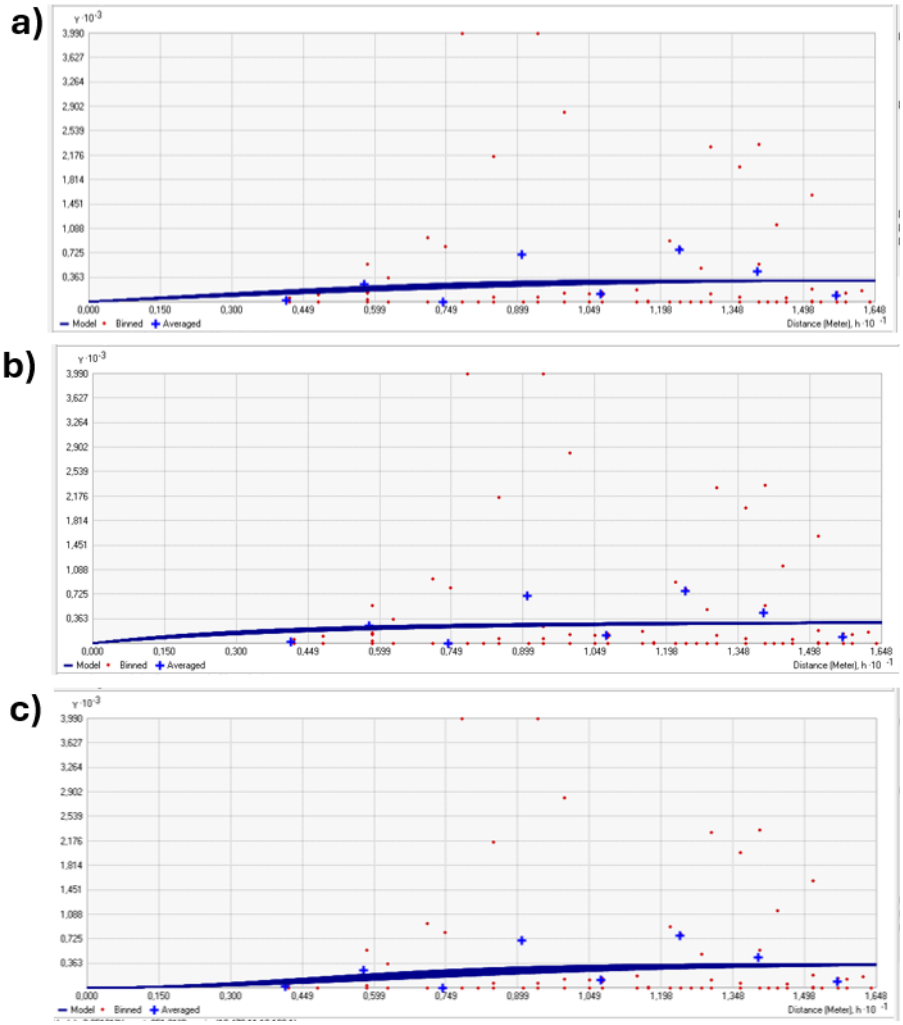


Figure 2. Fitting variogram model using Spherical (a), Exponential (b) and Gaussian (c)

All three semivariogram models exhibited relatively similar spatial structures, with a major range of 16.48 m and a minor range of 11.12 m, indicating that mercury concentrations remain spatially correlated over relatively short distances. Beyond this range, mercury concentrations become progressively independent, suggesting that contamination is predominantly controlled by localized historical mining activities rather than regional-scale environmental processes. This relatively limited spatial continuity is consistent with the localized use of elemental mercury during amalgamation, where contamination generally remains concentrated around former ore-processing facilities and tailings disposal areas.

The fitted semivariograms also revealed noticeable anisotropy, with the principal continuity oriented at approximately 121–128° depending on the selected model. The presence of anisotropy suggests that mercury dispersion was not spatially uniform but instead exhibited a preferred direction of continuity. Such directional dependence may reflect the combined influence of historical ore-processing layouts, surface runoff pathways, local drainage patterns, and terrain characteristics that controlled the redistribution of mercury following mining activities. Similar anisotropic behavior has been reported in contaminated mining landscapes where contaminant transport is influenced by topography and hydrological connectivity rather than isotropic diffusion alone. Directional spatial dependence has frequently been observed in heavy metal contamination studies because contaminant migration is commonly constrained by local geomorphological and hydrological conditions (Ersoy et al., 2008)

Among the evaluated models, the Gaussian semivariogram produced the lowest prediction error, with an RMSE of 13.96, compared with 15.56 for the Spherical model and 17.15 for the Exponential model

(Table 6). Among the three evaluated semivariogram models, the Gaussian model produced the lowest RMSE (13.96 mg kg^{-1}), compared with 15.56 mg kg^{-1} for the Spherical model and 17.15 mg kg^{-1} for the Exponential model. However, the magnitude of the Gaussian-model RMSE remained substantial relative to the mean Hg concentration of 10.18 mg kg^{-1}. Therefore, the Gaussian model was not considered highly reliable solely because it produced the lowest RMSE.

Model selection was instead evaluated using the complete set of cross-validation statistics, including mean error, mean standardized error, root mean square standardized error, and the relationship between observed and cross-validated predicted concentrations. The corresponding statistics are summarized in Table 6. Taken together, these diagnostics were used to determine whether the Gaussian model provided a comparatively better representation of the spatial structure than the alternative Spherical and Exponential models. Nevertheless, the relatively large prediction error indicates that quantitative concentration estimates, particularly around extreme Hg hotspots, should be interpreted with caution.

Table 6. Comparison of fitted semivariogram model parameters and prediction performance for mercury concentrations in soil.

Model	Main Direction (°)	Range		Nugget	Sill	RMSE
		Maj (m)	Min (m)			
Spherical	128	16.48	11.12	0	314.24	15.56
Exponential	121	16.48	11.12	0	313.4	17.15
Gaussian	128	16.48	11.12	0.35	351.2	13.96

An additional feature of the fitted semivariograms is the relatively small nugget effect. The Spherical and Exponential models produced nugget values close to zero, whereas the Gaussian model yielded a nugget of 0.35, which remains negligible compared with its total sill of 351.2. A low nugget-to-sill ratio generally indicates that measurement uncertainty and microscale variability contributed only minimally to the total spatial variance. Instead, most of the observed variability can be explained by structured spatial dependence associated with genuine environmental processes. This finding also provides indirect evidence that the sampling strategy and laboratory analyses were sufficiently consistent to capture the underlying spatial pattern of mercury contamination. The relatively large sill values observed for all three models primarily reflect the substantial variability in mercury concentrations across the study area. This variability is consistent with the descriptive statistical analysis presented in the previous section, which demonstrated a highly skewed distribution dominated by several extreme contamination hotspots. Consequently, the semivariogram captures both the localized enrichment resulting from historical amalgamation activities and the gradual decline in mercury concentrations away from these contamination sources.

Given the strongly right-skewed distribution of Hg concentrations, the stability of the spatial prediction was further evaluated using log-transformed data. As expected, transformation reduced the contrast between the highest Hg concentrations and the remaining observations and produced a smoother prediction surface. However, the principal contamination zone remained spatially associated with the same part of the former ASGM area, and the general pattern of decreasing Hg concentrations away from the main hotspot was preserved. Although the transformed model modified the magnitude and local smoothness of the predicted concentrations, it did not fundamentally alter the spatial interpretation of the contamination pattern. The raw-data Gaussian Ordinary Kriging model was therefore retained as the primary model because it preserves Hg concentrations in their original measurement units and maintains the magnitude of environmentally important hotspots. The transformed model was used as a sensitivity test to demonstrate that identification of the principal contamination zone was not solely an artifact of the extreme Hg values.

3.4 Spatial Distribution of Mercury Based on Ordinary Kriging

The spatial interpretation was restricted to the portion of the prediction surface adequately supported by the sampling locations. Because the 30 samples were purposively distributed around former mining, ore-processing, and potential runoff areas rather than uniformly across the entire mapped extent, predictions toward the peripheral parts of the original interpolation surface represent progressively greater extrapolation from measured observations. These peripheral predictions were therefore excluded from quantitative interpretation. The revised kriging map is restricted to the sampling-supported domain so that hotspot delineation is based primarily on areas constrained by observed Hg concentrations.

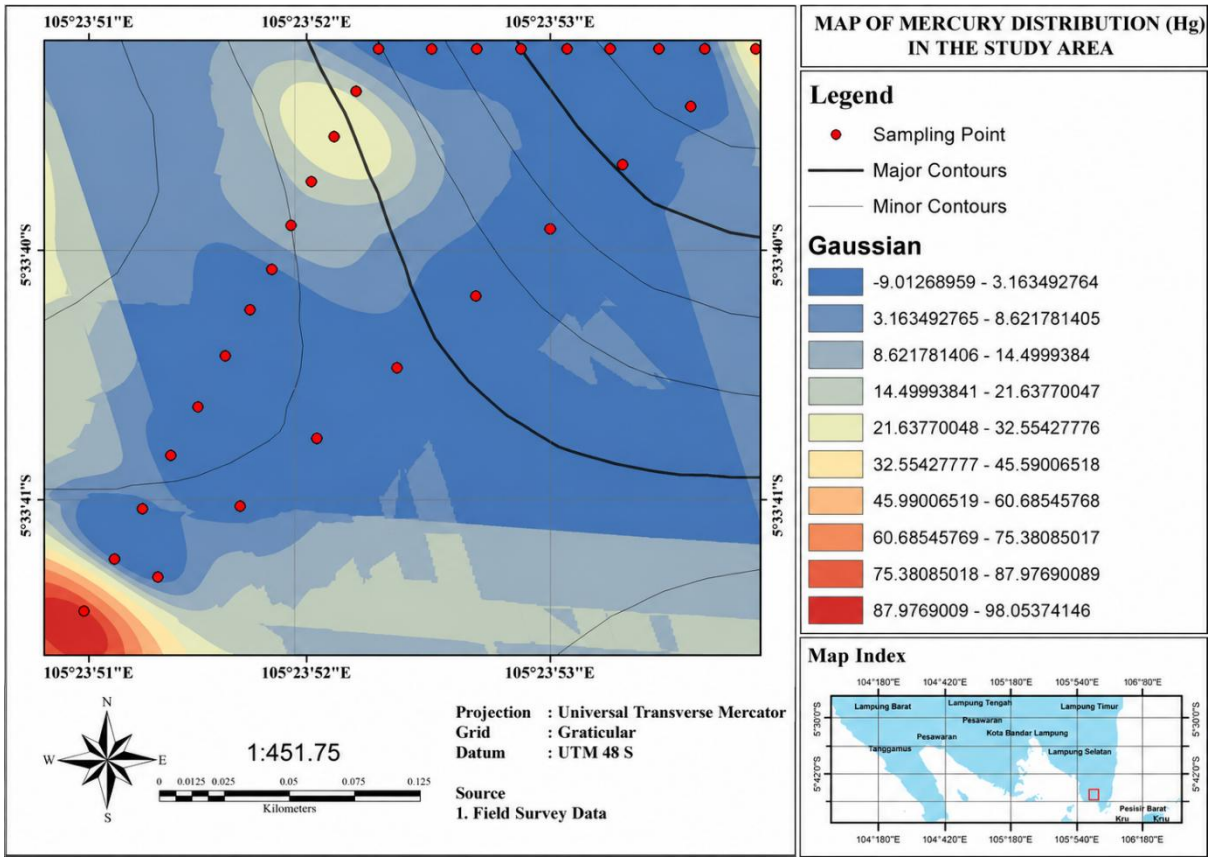


Figure 3. Spatial prediction of soil mercury concentrations generated using Ordinary Kriging with the Gaussian semivariogram model. The interpreted prediction surface is restricted to the spatial domain supported by the 30 sampling locations; areas outside this domain were excluded from interpretation to minimize unsupported extrapolation.

The highest predicted mercury concentrations were clustered within the central portion of the former ASGM site, corresponding to sampling locations that contained measured concentrations exceeding 30 mg kg^{-1} and reaching a maximum of 89.82 mg kg^{-1}. These localized areas most likely represent former amalgamation and ore-processing locations where elemental mercury was intentionally introduced during gold extraction. Because mercury was directly handled and discharged at these sites, substantial quantities remained within the surrounding soil, resulting in long-term residual contamination. Similar hotspot formation has frequently been reported in abandoned ASGM areas, where mercury contamination is strongly controlled by the spatial distribution of historical mining infrastructure rather than by natural geological variability. Localized mercury hotspots associated with former amalgamation and ore-processing areas have been consistently documented in post-mining environments worldwide, reflecting the concentrated use and release of mercury during historical gold extraction (Beckers and Rinklebe, 2017; Esdaile and Chalker, 2018; Kocman et al., 2013).

Away from these hotspot areas, predicted mercury concentrations declined rapidly over relatively short distances. This steep concentration gradient agrees well with the short spatial correlation range identified by semivariogram analysis (Section 3.3), indicating that mercury contamination decreases markedly beyond approximately 16 m from the principal contamination sources. The rapid decline in concentration also suggests that large-scale regional dispersion has been limited, whereas localized redistribution via runoff, soil erosion, and sediment transport has likely affected the immediate surroundings of the original contamination points. Consequently, the observed spatial pattern reflects both the legacy of historical mercury use and subsequent environmental redistribution processes operating at the local scale. The kriging map further demonstrates that areas exhibiting low mercury concentrations are interspersed between highly contaminated zones rather than forming continuous uncontaminated regions. This mosaic-like distribution indicates that contamination is spatially discontinuous, which is typical of abandoned ASGM landscapes where multiple ore-processing locations operated independently over time. Such discontinuous contamination patterns emphasize the importance of geostatistical interpolation, as conventional point-based sampling alone may fail to represent contaminant distribution between sampling locations adequately. By incorporating spatial autocorrelation. Within the sampling-supported spatial domain, Ordinary Kriging provides a continuous representation of the observed contamination pattern and facilitates the identification of potential Hg hotspot zones between sampled locations.

The cross-validation results indicate that the Gaussian model performed comparatively better than the Spherical and Exponential alternatives according to the evaluated prediction diagnostics. However, the relatively large prediction error, particularly in relation to the mean Hg concentration and the presence of several extreme observations, indicates that the interpolated concentrations should not be interpreted as precise site-wide estimates. Rather, the kriging surface is most appropriately used to identify the broad spatial pattern of contamination and potential hotspot zones that require further field verification and denser sampling.

3.5 Environmental Implications and Remediation Priority Assessment

The spatial distribution of mercury contamination identified in this study has important implications for environmental management and post-mining land restoration. Although mercury contamination was detected throughout much of the study area, the Ordinary Kriging interpolation indicated that most of the contaminant mass was concentrated in several localized hotspots. This finding suggests that mercury contamination is not uniformly distributed but instead remains closely associated with historical amalgamation and ore-processing activities. Consequently, remediation strategies should prioritize these hotspot areas to maximize environmental benefits while minimizing remediation costs.

The statistical analyses presented in Sections 3.1 and 3.2 further support this prioritization strategy. Although only 23.3% of the sampling locations were identified as statistical outliers, these locations contributed approximately 94.5% of the cumulative mercury inventory. Such disproportionate contamination indicates that a relatively small portion of the former mining area is responsible for the majority of the environmental mercury burden. From a remediation perspective, this concentration of contamination presents a significant opportunity for targeted intervention, as treating a limited number of highly contaminated sites may substantially reduce overall ecological risk.

Mercury contamination in these hotspot areas may pose multiple environmental risks because elemental mercury deposited during historical mining activities can undergo complex physicochemical transformations once it enters the soil environment. Under favorable environmental conditions, inorganic mercury may be converted into more mobile or bioavailable forms, increasing the potential for migration into surrounding ecosystems. Furthermore, mercury associated with fine soil particles may be transported through surface runoff during heavy rainfall events, resulting in secondary contamination of adjacent agricultural land, drainage channels, and surface water bodies. The long-term persistence and

environmental mobility of mercury remain among the primary ecological concerns associated with abandoned ASGM sites worldwide (United Nations Environment Programme, 2019)

Although the present study focused primarily on soil contamination, the identified hotspot areas may also represent potential sources of indirect human exposure. Communities living near former mining sites may be exposed through direct contact with contaminated soil, inhalation of contaminated dust during dry periods, or consumption of agricultural products cultivated in contaminated areas. In addition, mercury transported into nearby aquatic systems may enter local food webs via methylation, thereby increasing the potential for bioaccumulation in fish and other aquatic organisms. These exposure pathways emphasize the importance of integrating spatial contamination assessment with future ecological and human health risk evaluations. The kriging-derived contamination map provides a practical framework for establishing remediation priorities according to contamination severity and spatial distribution. Areas predicted to contain the highest mercury concentrations should receive immediate attention through detailed field verification and site-specific remediation planning. Intermediate contamination zones may require periodic environmental monitoring to evaluate potential contaminant migration, whereas areas with relatively low predicted mercury concentrations may primarily require long-term surveillance to ensure that contaminant redistribution does not occur over time. Such risk-based prioritization allows environmental resources to be allocated more efficiently than uniform remediation across the entire former mining site.

Several remediation technologies may be considered depending on the severity of contamination and site characteristics. Highly contaminated hotspots may require excavation and secure disposal or stabilization using mercury-binding amendments such as sulfur-containing materials or biochar. Moderately contaminated areas may be suitable for phytoremediation using mercury-tolerant plant species or assisted natural attenuation combined with long-term environmental monitoring. Selection of the most appropriate remediation strategy should consider not only mercury concentration but also land use, ecological sensitivity, accessibility, and potential human exposure pathways. Risk-based remediation has increasingly been recommended for former ASGM sites because contamination is commonly heterogeneous and localized rather than uniformly distributed (Brose and Heimberg, 2014; Kuppusamy et al., 2017).

The findings of this study also demonstrate the value of geostatistical analysis as a decision-support tool for contaminated land management. Rather than relying solely on discrete sampling results, Ordinary Kriging provides a continuous representation of contamination patterns that can support remediation planning, environmental monitoring, and regulatory decision-making. By integrating laboratory measurements with spatial prediction, environmental managers can identify priority intervention areas, optimize future sampling campaigns, and evaluate remediation effectiveness more efficiently than through conventional point-based assessments alone.

4. Conclusion

This study demonstrates that mercury contamination in the former ASGM area of Sidomekar Village, South Lampung, remains severe, spatially heterogeneous, and strongly controlled by localized historical mining activities. Aqua-regia-extractable Hg concentrations in surface soils ranged from 0.18 to 89.82 mg kg^{-1}, with a mean of 10.18 mg kg^{-1}. For descriptive comparison with the Indonesian soil environmental-health reference value of 0.30 mg kg^{-1}, 27 of the 30 samples (90%) were above this value. Because the analytical procedure quantified the aqua-regia-extractable fraction, this comparison should be interpreted as a screening-level assessment rather than a direct regulatory compliance determination. The large difference between the mean and median values, together with the high coefficient of variation, positive skewness, and high kurtosis, confirms that the contamination pattern is dominated by a limited number of extremely contaminated hotspots rather than by uniform site-wide pollution.

Geostatistical analysis further revealed that mercury concentrations exhibit strong short-range spatial dependence, with contamination patterns best represented by the Gaussian semivariogram model.

This model produced the lowest RMSE compared with the Spherical and Exponential models, indicating its suitability for Ordinary Kriging interpolation in this study area. The resulting kriging map successfully identified distinct mercury hotspots concentrated around former amalgamation and ore-processing zones, while also showing rapid concentration decreases away from these sources. These findings confirm that Ordinary Kriging is an effective spatial decision-support tool for identifying priority contamination zones in abandoned ASGM landscapes.

Overall, the results indicate that environmental management at the former ASGM site should focus on hotspot-based remediation rather than uniform treatment of the entire area. Because a small proportion of highly contaminated locations contributes disproportionately to the total mercury burden, targeted intervention in these zones could substantially reduce ecological and human exposure risks while improving remediation efficiency. Future work should include higher-density sampling around hotspot boundaries, assessment of mercury speciation and bioavailability, and integrated ecological and human health risk evaluations. The approach used in this study provides a practical framework for spatially informed monitoring, remediation planning, and sustainable post-mining land management in mercury-impacted ASGM areas.

Declaration of Generative AI and AI-Assisted Technologies in the Writing Process

During the preparation of this work, the author(s) used ChatGPT to improve the readability and fix grammatical errors. After using these tools/services, the author(s) reviewed and edited the content as needed and take(s) full responsibility for the content of the published article.

Acknowledgement

This study was funded by the Institute for Research and Community Service (Lembaga Penelitian dan Pengabdian kepada Masyarakat, LPPM) of the Institut Teknologi Sumatera.

Ethics Statement

This study did not require ethical clearance.

CRediT Author Statement

MAD, AFID: Conceptualization, formal analysis, funding acquisition, writing-review and editing. AJS, YTOS, MRS: Methodology, investigation, analysis. SBK: writing-review and editing.

References

Abdelaal, A., Sultan, M., Abotalib, A.Z., Bedair, M., Krishnamurthy, R.V. and Elhebiry, M. 2023. Emerging mercury and methylmercury contamination from new artisanal and small-scale gold mining along the Nile Valley, Egypt. Environmental Science and Pollution Research, 30(18), 52514–52534.

Becerra-Lira, E., Rodriguez-Achata, L., Muñoz Ushñahua, A., Corvera Gomringer, R., Thomas, E., Garate-Quispe, J., Hilares Vargas, L., Nascimento Herbay, P.R., Gamarra Miranda, L.A., Umpiérrez, E., Guerrero Barrantes, J.A., Pillaca, M., Cusi Auca, E., Peña Valdeiglesias, J., Russo, R., Del Castillo Torres, D. and Velasquez Ramírez, M.G. 2024. Spatio-temporal trends of mercury levels in alluvial gold mining spoils areas monitored between rainy and dry seasons in the Peruvian Amazon. Environmental Research, 245, 118073.

Beckers, F. and Rinklebe, J. 2017. Cycling of mercury in the environment: Sources, fate, and human health implications: A review. Critical Reviews in Environmental Science and Technology, 47(9), 693–794.

Boente, C., Albuquerque, M.T.D., Gerassis, S., Rodríguez-Valdés, E. and Gallego, J.R. 2019. A coupled multivariate statistics, geostatistical and machine-learning approach to address soil pollution in a prototypical Hg-mining site in a natural reserve. Chemosphere, 218, 767–777.

Brose, D. and Heimberg, J. 2014. Best practices for risk-informed decision making regarding contaminated sites: Summary of a Workshop Series (p. 18747). National Academies Press.

Cacciuttolo, C., Cano, D. and Custodio, M. 2023. Socio-environmental risks linked with mine tailings chemical composition: promoting responsible and safe mine tailings management considering copper and gold mining experiences from Chile and Peru. Toxics, 11(5), 462.

Carling, G.T., Diaz, X., Ponce, M., Perez, L., Nasimba, L., Pazmino, E., Rudd, A., Merugu, S., Fernandez, D.P., Gale, B.K. and Johnson, W.P. 2013. Particulate and dissolved trace element concentrations in three southern ecuador rivers impacted by artisanal gold mining. Water, Air, & Soil Pollution, 224(2), 1415.

Chen, C., Gao, M., Xiao, D., Mao, Y., Liu, J., Qiao, S. and Liu, J. 2026. Rice-mediated mercury exposure dominates human health risks in a legacy artisanal gold mining area of Southeastern China. Environmental Geochemistry and Health, 48(7), 316.

Danasla, M.A., Anjelita, C. and Julyanto, R.A. 2025. Phytoremediation as a Sustainable Solution for Mercury Contamination in Artisanal Gold Mining Sites: Insights from ASGM in South Lampung, Indonesia. Jurnal Presipitasi : Media Komunikasi Dan Pengembangan Teknik Lingkungan, 22(2), 432–447.

Dołęgowska, S. and Michalik, A. 2019. The use of a geostatistical model supported by multivariate analysis to assess the spatial distribution of mercury in soils from historical mining areas: Karczówka Mt., Miedzianka Mt., and Rudki (south-central Poland). Environmental Monitoring and Assessment, 191(5), 302.

Donkor, A.K., Ghoveisi, H. and Bonzongo, J.-C.J. 2024. Use of metallic mercury in artisanal gold mining by amalgamation: a review of temporal and spatial trends and environmental pollution. Minerals, 14(6), 555.

Eckley, C.S., Gilmour, C.C., Janssen, S., Luxton, T.P., Randall, P.M., Whalin, L. and Austin, C. 2020. The assessment and remediation of mercury contaminated sites: A review of current approaches. Science of The Total Environment, 707, 136031.

El Hadi, S.M., Abdeina, E.H., Chakiri, S., Baghdad, B. and El Hadi, H. 2026. Mercury contamination in soils and process waters near artisanal gold mining sites in Chami, Mauritania. Ecological Engineering & Environmental Technology, 27(5), 23–32.

Ersoy, A. and Yünsel, T.Y. 2018. The assessment of soil contamination by heavy metals using geostatistical sequential Gaussian simulation method. Human and Ecological Risk Assessment: An International Journal, 24(8), 2142–2161.

Ersoy, A., Yunsel, T.Y. and Atici, Ü. 2008. Geostatistical conditional simulation for the assessment of contaminated land by abandoned heavy metal mining. Environmental Toxicology, 23(1), 96–109.

Esdaile, L.J. and Chalker, J.M. 2018. The mercury problem in artisanal and small-scale gold mining. Chemistry – A European Journal, 24(27), 6905–6916.

Goovaerts, P. 1999. Geostatistics in soil science: State-of-the-art and perspectives. Geoderma, 89(1–2), 1–45.

Gosar, M., Šajn, R. and Teršič, T. 2016. Distribution pattern of mercury in the Slovenian soil: Geochemical mapping based on multiple geochemical datasets. Journal of Geochemical Exploration, 167, 38–48.

Imo, D., Dressel, H., Byber, K., Hitzke, C., Bopp, M., Maggi, M., Bose-O'Reilly, S., Held, L. and Muff, S. 2018. Predicted mercury soil concentrations from a kriging approach for improved human health risk assessment. International Journal of Environmental Research and Public Health, 15(7), 1326.

Kocman, D., Horvat, M., Pirrone, N. and Cinnirella, S. 2013. Contribution of contaminated sites to the global mercury budget. Environmental Research, 125, 160–170.

Kuppusamy, S., Venkateswarlu, K., Megharaj, M., Mayilswami, S. and Lee, Y.B. 2017. Risk-based remediation of polluted sites: A critical perspective. Chemosphere, 186, 607–615.

Moreno-Brush, M., McLagan, D.S. and Biester, H. 2020. Fate of mercury from artisanal and small-scale gold mining in tropical rivers: Hydrological and biogeochemical controls. A critical review. Critical

Reviews in Environmental Science and Technology, 50(5), 437–475.

Mulenga, M., Ouma, K.O., Monde, C. and Syampungani, S. 2024. Aquatic mercury pollution from artisanal and small-scale gold mining in sub-saharan africa: status, impacts, and interventions. Water, 16(5), 756.

Ngatijo, N., Permatasari, D.I., Farid, F., Bemis, R., Heriyanti, H., Basuki, R. and Wibowo, Y.G. 2021. Decontamination of mercury from mined soil using magnetite functionalized quaternary ammonium silica (Fe_3O_4/SAK). Jurnal Presipitasi : Media Komunikasi Dan Pengembangan Teknik Lingkungan, 18(1), 88–98.

Ridwan, Y.S., Koesmawati, T.A., Persulessy, A.E., Rosmalina, R.T., Sunaryani, A. and Dara, F. 2021. Mercury determination using stannous chloride reductant followed by atomic absorption spectrometric measurement: performance characteristics, uncertainty estimation, and compliance assessment. Jurnal Presipitasi : Media Komunikasi Dan Pengembangan Teknik Lingkungan, 18(2), 317–328.

Szponar, N., Vega, C.M., Gerson, J., McLagan, D.S., Pillaca, M., Delgado, S., Lee, D., Rahman, N., Fernandez, L.E., Bernhardt, E.S., Kiefer, A.M., Mitchell, C.P.J., Wania, F. and Bergquist, B.A. 2025. Tracing atmospheric mercury from artisanal and small-scale gold mining. Environmental Science & Technology, 59(10), 5021–5033.

Thiombane, M., De Vivo, B., Niane, B., Watts, M.J., Marriott, A.L. and Di Bonito, M. 2023. A new hazard assessment workflow to assess soil contamination from large and artisanal scale gold mining. Environmental Geochemistry and Health, 45(7), 5067–5091.

Uddin, S., Khanom, S. and Islam, Md. R. 2024. Source and distribution of mercury in environment—A Review. In N. Kumar (Ed.), Mercury Toxicity Mitigation: Sustainable Nexus Approach (pp. 3–43). Springer Nature Switzerland.

United Nations Environment Programme. 2019. Global Mercury Assessment 2018 (Technical Report Nos. 978-92-807-3744–8). https://wedocs.unep.org/handle/20.500.11822/27579

Wibowo, Y.G., Ramadan, B.S., Universitas Diponegoro, Maryani, A.T., Universitas Jambi, Rosarina, D., Universitas Muhammadiyah Tangerang, Arkham, L.O. and Institut Teknologi Sumatera. 2022. Impact of illegal gold mining in Jambi, Indonesia. Indonesian Mining Journal, 25(1), 29–40.

Yoshimura, A., Suemasu, K. and Veiga, M.M. 2021. Estimation of mercury losses and gold production by artisanal and small-scale gold mining (ASGM). Journal of Sustainable Metallurgy, 7(3), 1045–1059.